Relationships between Barrier Jet Heights, Orographic Precipitation Gradients, and Streamflow in the Northern Sierra Nevada

JESSICA D. LUNDQUIST

Department of Civil and Environmental Engineering, University of Washington, Seattle, Washington

JUSTIN R. MINDER

Department of Atmospheric Science, University of Washington, Seattle, Washington

PAUL J. NEIMAN

NOAA/Earth System Research Laboratory, Physical Sciences Division, Boulder, Colorado

ELLEN SUKOVICH

NOAA/Earth System Research Laboratory, Physical Sciences Division, and CIRES, University of Colorado, Boulder, Colorado

(Manuscript received 5 January 2010, in final form 19 May 2010)

ABSTRACT

The rate of precipitation increase with elevation, termed the orographic precipitation gradient (OPG), is critically important for hydrologic forecasting in mountain basins that receive both rain and snow. Here, the following are examined to see how well they are able to predict the OPG and how it changes between storms and years: 1) a linear model of orographic precipitation forced by upstream radiosonde data, 2) monthly Parameter-Elevation Regressions on Independent Slopes Model (PRISM) precipitation data, and 3) seven years of hourly wind profiler data used to identify characteristics of the Sierra barrier jet (SBJ). These are compared against 124 daily resolution (four of which also had quality controlled, hourly resolution) precipitation gauge records in the northern Sierra Nevada. All methods represent the OPG well in the mean and during a year when less than 30% of the precipitation occurred on days with SBJs. However, the linear model and PRISM do not adequately capture annual variations in the OPG during years when more than 70% of the precipitation occurred on days with SBJs. Throughout all of the years, wind profiler data indicating the height of the SBJ provided additional, and necessary, information. The OPG is negatively correlated with the height of the SBJ. The SBJ height is lower, and hence, the OPG greater when the westerly winds are stronger, with more vertical wind shear. These westerly storms result in greater increases of precipitation with elevation, which act to increase snow storage in most storms but also to increase storm runoff during warmer-than-average storms.

1. Introduction

The northern Sierra Nevada is a 3000-m-high, north–south-oriented mountain range subject to prevailing westerly winds, which exerts strong control on both the magnitude and distribution of precipitation in the region (e.g., Parish 1982; Marwitz 1983; Heggli and Rauber 1988; Pandey et al. 1999; Jeton et al. 1996; Dettinger et al. 2004; Galewsky and Sobel 2005; Reeves et al. 2008; Smith et al. 2010). Each year the majority of precipitation in northern California falls between November and April. Winter rains, on occasion, result in catastrophic floods [e.g., January 1995, described in Miller and Kim (1996); or January 1997, described in Galewsky and Sobel (2005)], while winter snowfall is essential for summer water supplies (e.g., Jeton et al. 1996). Because northern California basins span both rain- and snow-dominated elevations, the rate of precipitation increases with elevation, called the orographic precipitation gradient

Corresponding author address: Jessica D. Lundquist, Dept. of Civil and Environmental Engineering, University of Washington, Seattle, WA 98195-2700.
E-mail: jdlund@u.washington.edu

DOI: 10.1175/2010JHM1264.1

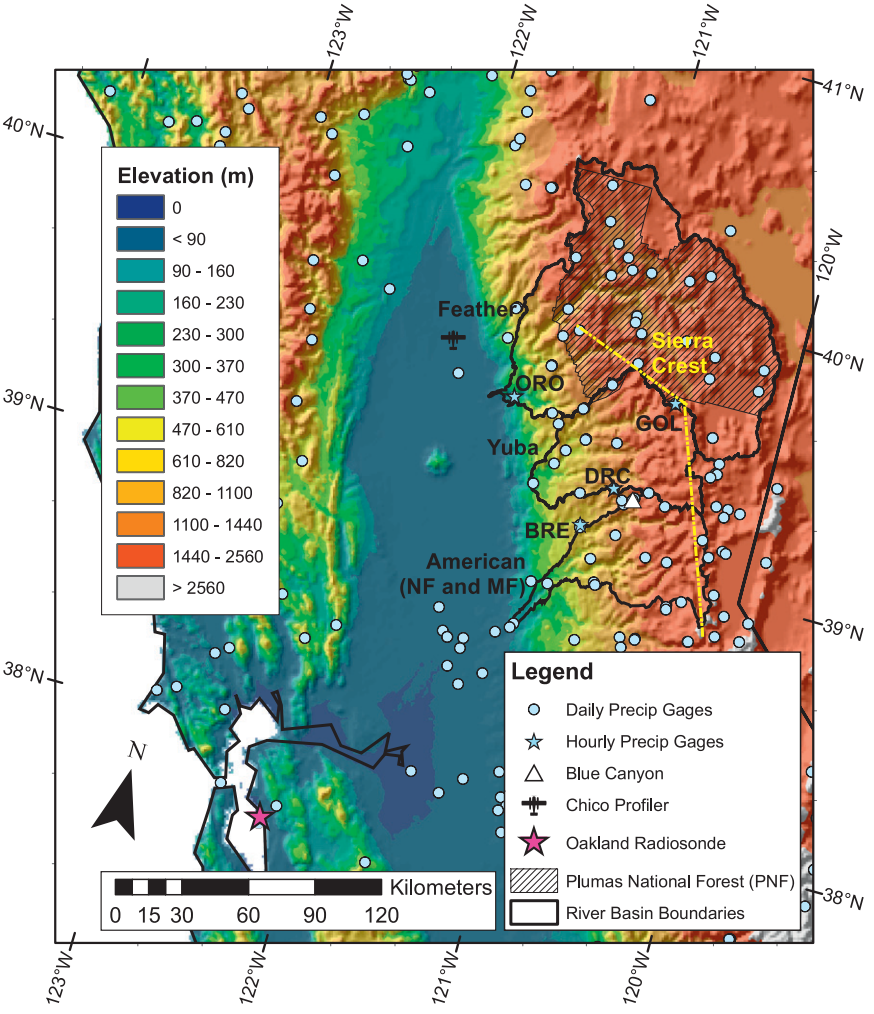

FIG. 1. Map of Sierra Nevada of California with the data sources used in this study. Feather, Yuba, and the American [encompassing the North and Middle Forks (NF and MF, respectively)] river basins are marked, as are the precipitation sensors examined in this study.

(OPG), is critically important (Dettinger et al. 2004; Lundquist et al. 2008). A greater OPG delivers a larger fraction of total precipitation as snow, which acts to delay the hydrograph, providing more runoff in the late summer and less in the winter (Dettinger et al. 2004). Thus, changes in OPGs may act to offset, or to exacerbate, projected climate change impacts for this region, such as more rain and less snow during the wet season (Knowles et al. 2006) and earlier snowmelt (Stewart et al. 2005).

The National Oceanic and Atmospheric Administration's Hydrometeorological Test Bed (NOAA/HMT; Ralph et al. 2005) is a long-term national campaign designed to transition state-of-the-art research into National Weather Service (NWS) and River Forecast Center (RFC) operations and has focused on the northern Sierra Nevada since 2001 (Fig. 1). HMT has supported the unique observational dataset used in this study with the specific goal of accelerating research and development and enhancing the infusion of research into forecasting operations. Hydrologic forecasts generally rely on point measurements to estimate precipitation across an entire watershed. The translation from point to area is generally based on regression, using the historic record of precipitation and streamflow to determine the average relationship between a reference gauge, or gauges, and the basin area of interest. For example, the California Department of Water Resources (CADWR; more information available online at www.water.ca.gov) uses a regression equation relating 12 snow-pillow measurements to forecast summer runoff in the Feather River basin (a basin area of 5185 km^2, or 1 measurement per 432 km^2), which supplies the largest reservoir for the California State Water Project. In the southern Sierra Nevada, where even fewer stations exist, streamflow

forecasts often rely on just one precipitation measurement per basin. This regression method works well so long as the actual spatial pattern of precipitation is similar to the mean spatial precipitation pattern. During periods when the spatial pattern of precipitation differs substantially from the long-term mean, large forecast errors can result.

This paper examines the average precipitation pattern and deviations from the long-term mean pattern for the northern Sierra Nevada for the period 2001 to 2007, during which a key HMT wind-profiler dataset from Chico was available, as were additional HMT observational datasets. These datasets allow us to investigate patterns of precipitation at high spatial and temporal resolution and to look at characteristics of the atmospheric flow that impinge on the mountains and act to modify precipitation patterns. First, we investigate how well variations in precipitation patterns can be represented using observations from Oakland soundings (Fig. 1) combined with an idealized linear model of orographic precipitation (Smith and Barstad 2004), as well as by a geostatistical model for interpolating between station observations [Parameter-Elevation Regressions on Independent Slopes Model (PRISM); Daly et al. 1994]. Second, we examine how processes not included in the idealized model, specifically blocking as characterized by the Sierra barrier jet (SBJ), relate to spatial patterns of precipitation. Finally, we discuss implications for basin hydrology. Throughout the paper, we discuss spatial patterns but particular emphasis is put on variations in precipitation accumulation with elevation, since this has the greatest impact on magnitudes of rain versus snow and, thus, on flood magnitudes and summer water supply stores (Dettinger et al. 2004).

2. Factors controlling precipitation patterns in the Sierra Nevada

Mountains modify weather systems by forcing air parcels to rise above or divert around them (see Smith 1979; Barros and Lettenmaier 1994; Roe 2005 for reviews). A saturated parcel of air will condense at a rate close to the rate of change of the saturated moisture content (e.g., Houze 1993; Roe 2005),

$$C = -\frac{\partial(\rho q^{\text{sat}})}{\partial z}\frac{dz}{dt}, \tag{1}$$

where C is the condensation rate, ρ is the air density, z is height, t is time, and q^{sat} is the saturation-specific humidity. Assuming airflow is steady, uniform with height, and parallel to the topography at all heights, the change in air parcel height with time (dz/dt) is a function of the slope of the terrain and the velocity of the air impinging upon the slope. Therefore, integrating Eq. (1) from the surface to the top of the atmosphere and assuming all condensed droplets immediately fall out as precipitation, the resulting precipitation rate is proportional to the terrain-perpendicular moisture flux and the slope of the terrain over which the air parcel is forced, with a maximum accumulated precipitation over the steepest windward slopes (e.g., Smith 1979; Alpert 1986; Roe and Baker 2006). Models taking this approach are termed "slab models" because they assume that air flows as a uniform slab over the terrain.

Although numerous studies have used these basic assumptions to model precipitation distributions in mountain ranges (e.g., Sawyer 1956; Colton 1976; Rhea 1978; Alpert 1986; Pandey et al. 1999; Alpert and Shafir 1989; Sinclair 1994; Roe 2002; Smith and Barstad 2004), precipitation distributions are better represented by modeling the growth and downwind advection of hydrometeors, which has been accomplished in linear models with simple, tunable parameters (e.g., Barros and Lettenmaier 1993; Smith 2003; Smith and Barstad 2004, Roe and Baker 2006). Barros and Lettenmaier (1993) and Smith and Barstad (2004) also incorporated mountain wave dynamics, by allowing the vertical velocity to vary with altitude according to linear Boussinesq mountain wave theory (e.g., Queney 1947; Smith 1979, 2002). This addition allows the precipitation rates and structure to vary depending on how the moist static stability (Durran and Klemp 1982) compares to the advection frequency. For narrow mountains, low stability, and/or strong winds, gravity waves dampen with height, and lifting occurs through a limited vertical extent. In these cases, maximum condensation rates are reduced, but still maximize over the windward slopes (Smith and Barstad 2004). For high stabilities, low wind speeds, and wide mountains, gravity waves propagate vertically and tilt upstream with height, resulting in lifting and condensation upwind of the mountains, and more precipitation at lower elevations. Thus, the latter case may result in a weaker OPG.

While the atmospheric stability can vary the OPG through linear wave dynamics, it can also be important for determining the extent of terrain blocking (Pierrehumbert and Wyman 1985), a processes not represented with linear dynamics (Smith and Barstad 2004). Blocking occurs when a stable air mass impinges upon a mountain, slows down, and is unable to surmount the barrier. Slower velocities weaken the Coriolis force, and the blocked airflow turns to the left of its direction of motion in the Northern Hemisphere, resulting in flow parallel to the mountain range (Reiter 1963; Shutts 1998; Petersen et al. 2005; Barry 2008). Along a north–south mountain barrier, with storms impinging from the west, this results in southerly

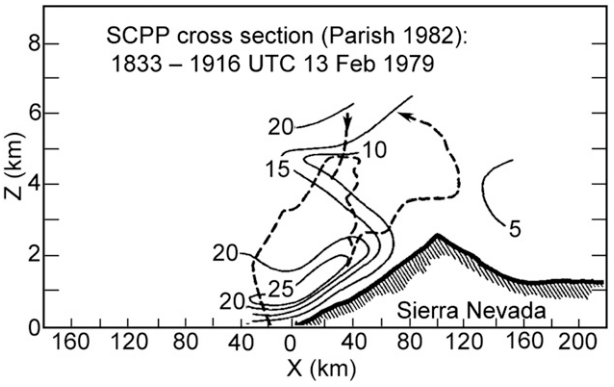

FIG. 2. Illustration of barrier jet along the Sierra Nevada, taken from Parish (1982). Dashed line indicates the aircraft flight track, and solid contours indicate mountain parallel wind velocities derived from rawinsonde and aircraft data on 13 Feb 1979.

flow. The region of maximum terrain-parallel velocity in this layer of blocked flow is termed the barrier jet, which was first identified during the Sierra Cooperative Pilot Project (SCPP) experiment in northern California (Parish 1982; Fig. 2) and later described by Marwitz (1983), Smutz (1986), and Neiman et al. (2010), among others. Similar SBJ flows have been observed in many mountain ranges (e.g., Rocky Mountains, Dunn 1992; Alps, Rotunno and Ferretti 2001; California Coast Range, Neiman et al. 2002; Valdez–Cordova mountains of Alaska, Loescher et al. 2006), thus the understanding gained in the Sierra Nevada is applicable to many regions.

Hughes et al. (2009), focusing on Southern California, found that blocking was the main cause of precipitation patterns deviating from that predicted by a Smith and Barstad (2004) linear model. Leung and Ghan (1995, 1998) and Leung et al. (1996) parameterized blocking in their subgrid orographic precipitation scheme in hydroclimate simulations and found that their subgrid scheme improved overall model performance. In general, blocking is associated with increased precipitation upstream of the mountain range and decreased precipitation over the upper windward slope (Neiman et al. 2002; Colle 2004; Galewsky 2008), although forced ascent of the SBJ at the northern end of California's Central Valley frequently results in enhanced precipitation in that area (Reeves et al. 2008).

Varying precipitation patterns may also arise from other mountain–storm interactions. For example, vertical wind shear may alter the mountain wave structure (e.g., Smith 1989; Colle and Mass 1998), generate turbulence and updraft cells (Houze and Medina 2005; Medina et al. 2005), and/or alter the microphysical time scales aloft (e.g., Jiang and Smith 2003). These processes, in turn, alter the precipitation distribution (Colle 2004). Based on idealized two-dimensional simulations with a mesoscale model, Colle (2004) found that increasing wind speeds with height (forward wind shear) moved the precipitation maximum closer to the crest, while backward wind shear shifted the precipitation maximum farther upstream (downslope) from the mountain crest.

Isolated regions of heavy precipitation also result from the convergence of adjacent air masses that interact differently with the topography. For instance, drier air may be blocked by a mountain range and diverted along the topography, while at the same time, a moister adjacent air mass may be accompanied by enough latent heat release to increase its buoyancy, allowing it to flow over the topography. Localized precipitation maxima can occur where these air masses converge (Rotunno and Ferretti 2001; Galewsky and Sobel 2005; Reeves et al. 2008).

Here, we seek to answer two primary questions related to variations in orographic precipitation gradients in the northern Sierra Nevada: 1) Can the salient patterns be explained by upstream airflow conditions as predicted by linear theory, or by monthly PRISM maps of precipitation? If so, at what aggregate time scale: multiyear average or annual? 2) How much more information do we gain by considering nonlinear dynamics, specifically, the SBJ structure, which can be observed with a vertical wind profiler? Section 3 describes the methods, data, and models used. Section 4 shows how a linear model of orographic precipitation and PRISM represent the mean well, but cannot adequately capture annual variations in the OPG. Section 5 demonstrates how the height of the SBJ relates to the OPG. Section 6 looks at hydrologic sensitivity; section 7 summarizes the results; and section 8 discusses possible explanations for these patterns.

3. Datasets and methods

a. Surface precipitation observations

Daily precipitation data were obtained from the California Department of Water Resources and cooperating agencies, who manage a network of 124 precipitation gauges in or near the Feather, Yuba, and American river basins (Fig. 1; data available at http://cdec.water.ca.gov). Low-elevation sites consisted of both tipping-bucket and accumulation reservoir gauges, while most high-elevation sites in the region were precipitation reservoir gauges with antifreeze. For finescale analysis, hourly data were obtained from four CADWR stations on the west slope of the study area from October 2001 to September 2007 (Table 1) and were carefully quality controlled by visual inspection.

Based on data availability, subsets of these data were ingested into the PRISM (available at http://www.prism.oregonstate.edu) to produce monthly quantitative precipitation estimation (QPE) maps for water years 2001 to 2007 at 4-km resolution (Daly et al. 1994, 2002, 2008).

TABLE 1. Hourly observation stations.

Station Name	Station ID	Elevation (m)	Latitude (°N)	Longitude (°W)
Bear River at Rollins Reservoir	BRE	593	39.1330	120.9530
Gold Lake	GOL	2057	39.6750	120.6150
Deer Creek	DRC	1358	39.3000	120.8250
Oroville Dam	ORO	274	39.5400	121.4930

Each water year contains the sum of all precipitation from 1 October of the prior year through 30 September. Average patterns over 1980 to 2007 were also examined and were similar to the shorter time period shown here. PRISM uses empirical relationships to account for the influence of elevation, rain shadows, and coastal proximity when interpolating between existing measurement stations. All available station data goes into creating PRISM long-term climate normals, but the monthly product uses climatology for interpolation at places and times with missing data (C. Daly 2009, personal communication).

b. *Atmospheric observations: Radiosonde and wind profiler*

Upper-air measurements of temperature, dewpoint temperature, wind speed, and wind direction were obtained from the National Weather Service radiosonde network site at Oakland, California (OAK; location shown in Fig. 1), at 0000 and 1200 UTC (0400 and 1600 PST) each day. This site is generally upwind of the study area and represents free-air conditions before the air encounters the topography of the Sierras.

The characterization and time series of SBJ parameters used here are described in detail in Neiman et al. (2010). Here we focus on data collected from 2 June 2000 to 7 May 2001 and from 11 November 2001 to 23 May 2007 using an all-weather 915-MHz radar wind profiler (e.g., Martner et al. 1993; Carter et al. 1995) located at Chico in the northern Central Valley at 41-m elevation (Fig. 1). The wind profiler analyses in Neiman et al. (2010) are based on a terrain-relative coordinate system, whereby the axes are rotated 20° counterclockwise from the cardinal directions (i.e., the positive V component of the flow aligns with the long axis of the Sierra Nevada from 160° to 340°). Objective barrier-jet criteria were applied to the hourly V-component profiles as follows. A relative maximum in V of at least 12 m s^{-1} was required between the profiler's second range gate (~200 m above ground) and 3 km MSL (i.e., below crest level). In addition, the V component must have decreased by more than 2 m s^{-1} with increasing height somewhere between the core altitude of the SBJ and 3 km MSL. If more than one relative maximum were observed, the maximum with the greatest V was taken as the SBJ. An SBJ case was defined as a group of at least eight consecutive hourly wind profiles with SBJ attributes.

c. *Linear model of orographic precipitation*

To test how the bulk wind speed and direction, temperature and stability, along with the topography, affect the mean precipitation pattern and variations from the mean, we ran a model based on the linear theory (LT) model of orographic precipitation (Smith and Barstad 2004). The LT model, when properly calibrated, has performed well in many climatological applications (e.g., Smith et al. 2003; Barstad and Smith 2005; Anders et al. 2007; Crochet et al. 2007; Minder 2010). It solves for the steady-state condensation, advection, fallout, and evaporation of water occurring in vertically integrated atmospheric columns for a horizontally and vertically uniform airstream impinging on the mountain range. The LT model solves the linearized equations of motion for flow over topography (Smith 1979) and accounts for the finite times required 1) for cloud water to convert into precipitation and 2) for precipitation to fall to the ground. The model assumes stable stratification and saturated conditions. The model neglects potentially important processes, such as post-cold-frontal convective precipitation and terrain blocking.

The LT model was run (as in Minder 2010) by prescribing characteristic winds (speed and direction), stratification (moist stability, N_m^2), and low-level temperatures based on rawinsonde measurements collected at Oakland between water years 2000 and 2007. Conditions likely to correspond to mountain precipitation events were isolated by picking out ''storm'' soundings, defined as soundings in which the 1- to 3-km layer had an average relative humidity (RH) greater than 75%. The temperature forcing came from the average of the interpolated 100- to 200-m layers in the sounding, and wind and moist stability parameters were calculated from the 1- to 3-km layer (details in Minder 2010). Two microphysical time delay constants (τ_c and τ_f, representing time scales for the conversion of cloud to precipitation and fallout, respectively) were each set to 2200 s. We examined time delay parameters ranging from 850 to 2800 s and found that the time delay primarily changed the curvature of precipitation versus elevation, with smaller delays greatly increasing precipitation at the lowest mountain elevations while decreasing precipitation at higher mountain elevations. We chose the time constant that resulted in a mean pattern of precipitation that best matched observations. The background precipitation rate (representative of precipitation generated directly by synoptic storms) was also tuned to match climatological precipitation observations (as in Minder 2010).

d. Hydrologic model

To test the effects of precipitation distributions on basin hydrology, we developed a simple model of the Yuba River basin (outlined in Fig. 1). The basin was broken into 24 elevation bands from 200 to 2500 m, each spanning 100 m of elevation. Reference precipitation, taken as the average of precipitation at all stations below 200 m, was used to estimate precipitation across the basin for four different precipitation scenarios, which are described in section 6. For all scenarios, daily temperature was measured at Blue Canyon (Fig. 1; 1610-m elevation) and distributed to each elevation band using a moist adiabatic lapse rate of $-6.5°C\ km^{-1}$.

Daily temperature and precipitation in each elevation band were used to drive Snow-17 (Anderson 1973), a snow model used for operational weather forecasting. Snow-17 identifies precipitation as rain ($T > 1°C$) or snow ($T < 1°C$) and uses an energy-balance approach to accumulate or melt snow during rain-on-snow events and a degree-day approach to melt snow during nonrain events. Model outflow was the daily sum of liquid precipitation passing through the snowpack and snowmelt. At each elevation band, model outflow was first weighted by the total basin area within that elevation band, and then the sum of the weighted outflows from all elevation bands was fed through a linear reservoir model to derive streamflow. The linear reservoir model performs a convolution interval of the snow model outflow with a response function, $h/\Sigma h$, where $h = \exp(-0.0319t)$ and t is computed in days from 1 to 18, following the formulation of Dooge (1973). The model is designed to illustrate how changes in precipitation distributions affect runoff in a mountain environment that spans both rain and snow elevation zones. Therefore, the model does not include any representation of evaporation, soil water storage, or other water losses, nor does it account for basin characteristics, aside from a snowpack, that might change runoff characteristics throughout the year.

4. Results: How well can linear theory and PRISM predict spatial precipitation patterns?

Dettinger et al. (2004) found that the greatest OPGs in the Sierras occurred when storms transported water vapor from a nearly westerly direction, as opposed to a southwesterly direction, which often resulted in greater total precipitation amounts. Dettinger et al. (2004) suggested that their observational results locally confirm linear models of precipitation, specifically models used by Rhea and Grant (1974) and Hay and McCabe (1998). Although the transport direction was the dominant variable, which can be explained with a simple upslope slab model, greater precipitation gradients were also associated with less stable airflows, a result not predicted by slab models.

Figure 3 presents spatial maps and elevation profiles (focused on the Yuba basin for the gridded datasets and on stations falling within the marked box for gauge data) of mean annual precipitation over water years 2001 to 2007. The median elevation profile for the 1980 to 2007 PRISM mean is also shown (dash–dot line) for reference. Compared to PRISM output and station observations, the LT model overestimates the mean annual precipitation in the northwest and southeast edges of the northern Sierra domain but otherwise represents the average spatial patterns of precipitation well. PRISM, gauge observations, and the LT model all show a precipitation maximum at middle elevations on the westward slope, and the greatest precipitation magnitudes in the western portion of the Plumas National Forest (PNF; shown in Fig. 1) of the Feather River basin. On average, the LT model estimates 12% more precipitation in the basin than PRISM, with a greater degree of overestimation at lower elevations and a slight underestimation at the highest elevations. Both the LT model and PRISM exhibit patterns of increasing precipitation with elevation to approximately 1000 m (a region covering about 35% of the total watershed area) and then nearly constant precipitation from 1000 m to the basin ridgeline (2500 m). Above 1750 m, the LT model shows a slight decrease in precipitation as height increases. Typically, gauge observations of precipitation are less than either PRISM or the LT model, but this may be due to gauge undercatch. The gauge data have sparse coverage above 1100 m. Thus, the gauge data may indicate a linear increase in precipitation at all elevations, with increasing scatter at higher elevations, or an increase in precipitation to 1000 m, with no change but high variability above that elevation.

To further compare the model results with observations, hourly precipitation data at four stations (Table 1) were summed over the 12-h following each sounding used to force the LT model. The LT model was able to generally capture variations in the OPG associated with changes in westerly wind speed (Fig. 4a) and stability (Fig. 4b).

To examine how well the LT model and PRISM capture year-to-year variations in the OPG, the annual accumulated precipitation is plotted as a function of elevation (Fig. 5) for the boxed region in Fig. 3c. For PRISM and the LT model, only median values are shown for each elevation band. Based on visual inspection, the models all capture the year-to-year variation in precipitation, with fairly good agreement at the lowest elevations (Fig. 5). However, they represent the OPG much better in some years (e.g., 2001 and 2003) than in

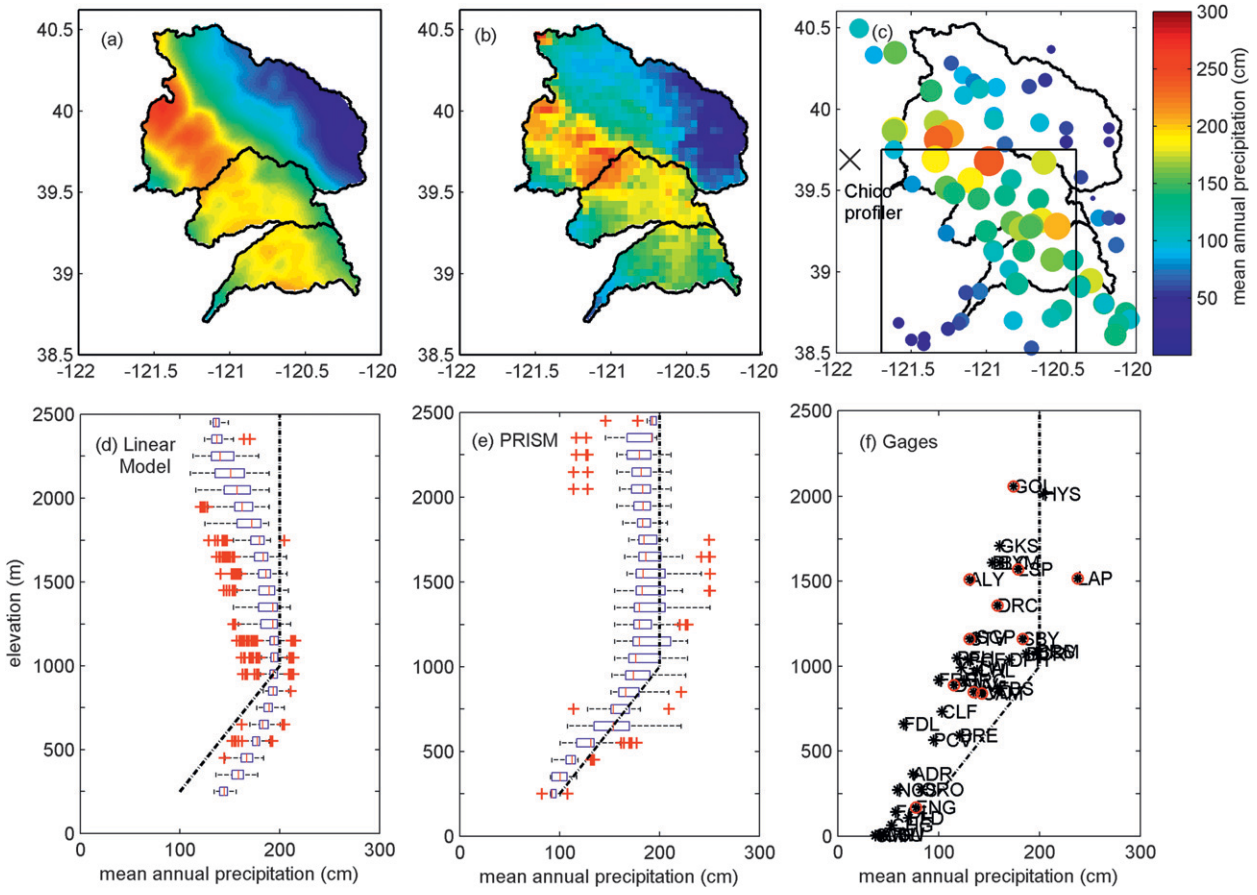

FIG. 3. Average water-year precipitation accumulation (cm) for water years from 2001 to 2007, for (a),(d) simulations with the LT model forced with Oakland sounding information, (b),(e) 4-km resolution PRISM maps of interpolated surface precipitation measurements, and (c),(f) precipitation gauges. Black basin boundaries are as in Fig. 1. Box and whisker plots of mean annual precipitation (MAP) in centimeters for each 100-m elevation band within the Yuba basin for (d) the LT model, (e) PRISM, and (f) station observations, where red circled dots are stations within the Yuba basin, and black dots are stations in neighboring basins. In (d) and (e), the left and right edges of each blue box are the 25th and 75th percentiles of the MAP, respectively, and the width of the box is the interquartile range. The red line is the median. The horizontal black dashed lines or ''whiskers'' illustrate the extent of other values, except for those that are more than 1.5 times the interquartile range away from the edges of the blue box, which are displayed with a red +. The black dash–dot lines indicate the approximate 1980 to 2007 PRISM average for the region: an increase of precipitation from 100 to 200 cm between 250- and 1000-m elevation, with constant 200 cm precipitation above, for reference.

others (e.g., 2002, 2006, and 2007). This suggests that processes other than those captured by the LT model have important influences on precipitation distributions, and these influences aggregate to the annual time scale.

5. Results: Influence of barrier jets on spatial precipitation patterns

One phenomenon absent from the LT model, but recognized as affecting Sierra precipitation patterns, is the SBJ (e.g., Marwitz 1983; Smutz 1986; Neiman et al. 2010). The potential importance of the SBJ depends on the percentage of total annual precipitation that occurs during the presence of an SBJ. Using hourly observations, Neiman et al. (2010) calculated the precipitation that fell during SBJ cases compared to during non-SBJ cases for three stations near the Chico, California, wind profiler and found that 55%, 56%, and 47% of the total precipitation at stations at elevations of 70, 488, and 1570 m, respectively, fell during recognized SBJ conditions.

To expand over a greater region, we identified 43 stations within the bounding limits of 38.5° to 39.75°N and 121.7° to 120.4°W (chosen to isolate west-slope stations) for the period of 1 October 2000 to 30 September 2007, focusing on the months of October through May, as this was the period when the profiler was operational and SBJ information is available. However, because little precipitation falls in the warm season, the statistics did not change when total water-year precipitation was used instead. Start and stop times of observed SBJ cases were

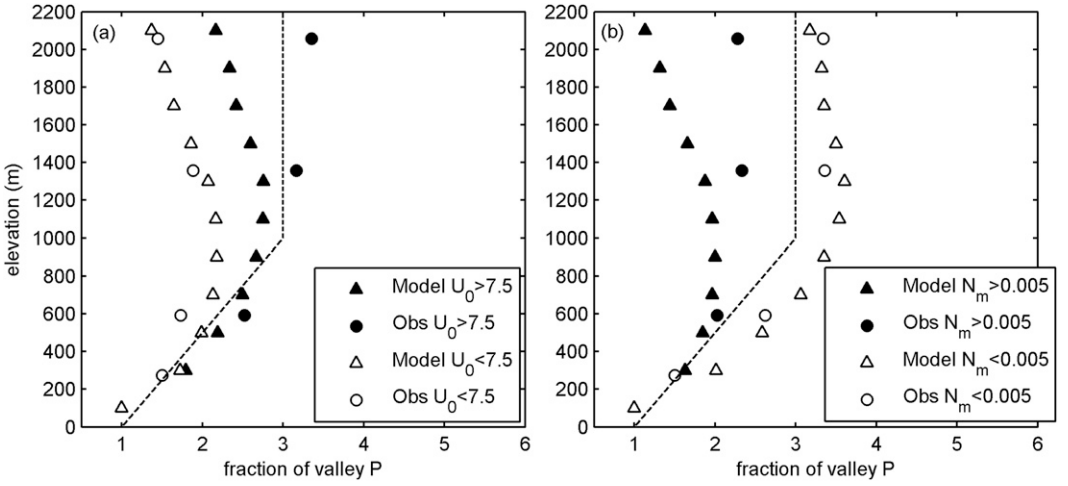

FIG. 4. Average precipitation weights for elevation-binned LT model output and for hourly precipitation observations for all events from 2000 to 2007 that satisfied the criteria to run the LT model (RH > 75%), binned by (a) westerly wind speed greater than and less than 7.5 m s^{-1} and (b) moist static stability greater than and less than 0.005 s^{-1}.

averaged to the nearest whole day, using local standard time.

Over the entire period, daily precipitation on days with an identified SBJ case made up approximately 64% of the total October to May measured precipitation, with a standard deviation of 9%. This daily derived value is larger than that tabulated by Neiman et al. (2010), who used hourly precipitation, because often substantial precipitation amounts occurred in the hours just after the end of the SBJ.

To examine the effect of daily resolution on these fractions, we obtained hourly precipitation records for four stations for the period of interest (Table 1). For these stations, only 30% ± 1% of the total precipitation accumulated during the hours of an SBJ, compared to 62% ± 1% that accumulated on the same day as an observed SBJ. The fraction of total annual precipitation that occurred during hours with SBJ conditions was generally about half of the fraction of annual precipitation

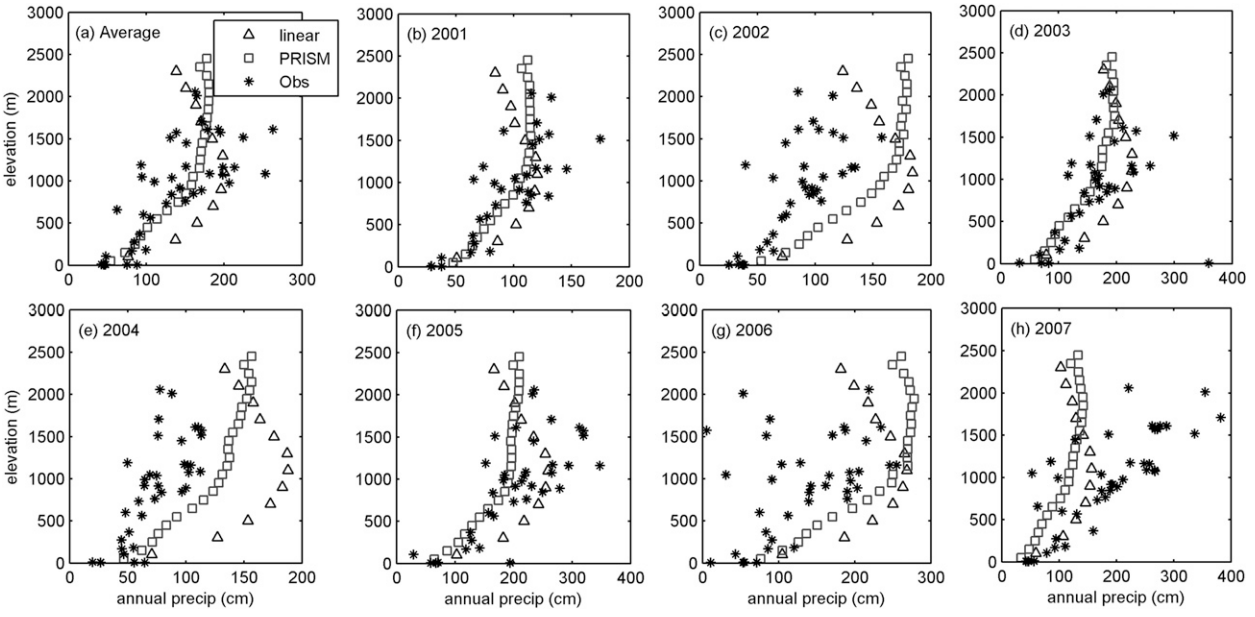

FIG. 5. Annual precipitation accumulation for the same data as shown in Fig. 3 for (a) the median of all elevations for the mean of water years from 2001 to 2007, and (b)–(h) the median for each water year.

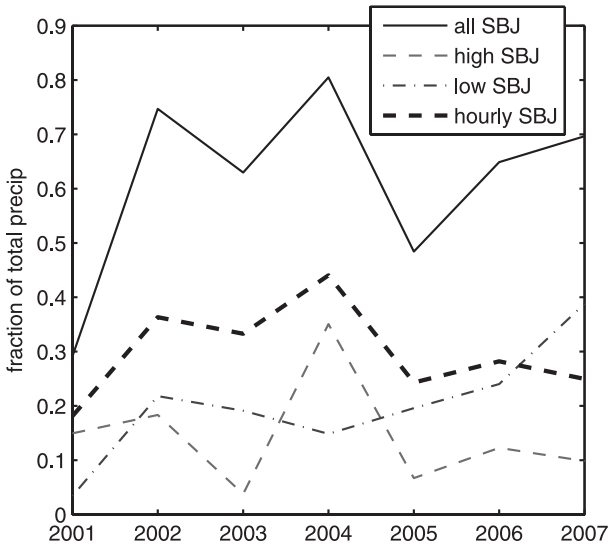

FIG. 6. Fraction of total October to May precipitation falling on days with a recognized barrier jet (all SBJ), with a barrier jet containing a core altitude >1200 m MSL (high SBJ) and a core altitude <700 m MSL (low SBJ), based on daily precipitation data at 43 stations in the central region of the study area. Fraction of October to May precipitation falling during hours with a recognized barrier jet (hourly SBJ) is based on four stations (Table 1).

occurring during days with SBJ conditions. Thus, while the actual fraction of annual precipitation attributed to SBJ conditions depended on the resolution of the data examined; the interannual variations, that is, years with high versus low fractions of total precipitation attributable to SBJ-associated storms, were similar regardless of the time step examined (Fig. 6).

The water year ending in 2001 was anomalous compared to the others, with ~30% of the annual precipitation occurring on days when SBJs were observed (Fig. 6). In contrast, between 50% and 80% of the annual precipitation in water years 2002 to 2007 occurred on days with recognized SBJ conditions. The water years of 2002, 2004, and 2007 all had over 70% of precipitation occur on days with SBJs, and these same years had particularly large variations in the OPGs reported by PRISM, the LT model, and observations (Figs. 5c,e,h). Of the seven-year period examined, 2001 had the best agreement between the three data sources, suggesting that the LT model and PRISM may work best in years with limited influences from SBJ conditions.

Neiman et al. (2010) classified SBJs observed during the 2000–07 observation period as "strong versus weak velocity," "long versus short duration," and "high versus low altitude," with all terms referring to the jet's core wind speed directed from 160° to 340° (i.e., parallel to the mountain range). We examined precipitation distributions in all of these cases and found that while the strong and long SBJs had considerably more precipitation magnitude than the weak and short SBJs, the patterns of precipitation distribution were remarkably similar between the two categories (not shown). In contrast, the altitude of the SBJ exerted a strong control on precipitation patterns. Therefore, the following examines the altitude of the SBJ relative to precipitation patterns.

High SBJs were classified as those with core altitudes greater than 1200 m, and low SBJs as those with core altitudes less than 700 m. These altitude cutoffs were selected such that the identified high- and low-altitude SBJs each made up about one-third of the total SBJ-associated precipitation, with the remaining third in the middle. Figure 7 illustrates the mean precipitation measured at all gauges within the domain on days with low and high SBJs. The low-elevation stations of the Central Valley (southwest corner of the domain) exhibit little variation between the SBJ types. Thus, any precipitation map based on weights relative to these low-elevation stations would predict similar rates of precipitation across the domain. However, the daily precipitation rates at higher elevations are approximately twice as large during low SBJs (Fig. 7a) than during high SBJs (Fig. 7b). This precipitation increase is correlated with elevation and focused on the west slopes of the Sierra Nevada to the southeast of the Chico profiler. To further analyze this pattern, we selected the subset of stations shown in the box drawn on Fig. 7. This subset excludes stations in the rain shadow of the Sierra crest and focuses on the region where the Sierra topography is simplest, essentially a slab increasing in elevation from southwest to northeast. This box defines the same 43 stations used for the statistics in Fig. 6.

Using this subset of stations, we analyzed the precipitation as a function of elevation, because of the importance of elevational patterns for hydrology. Because precipitation at higher elevations is generally determined relative to a reference precipitation at low altitude, P_0 is defined as the reference precipitation rate, which is taken as the average of the eight stations in the domain at elevations less than 200 m.

$$P(z) = P_0 + \alpha P_0 z, \quad \text{or} \quad \frac{P(z)}{P_0} = 1 + \alpha z, \qquad (2)$$

where z is elevation, and α is a measure of the OPG. For all days with greater than 5 mm mean regional precipitation, $\alpha = 1.5\ \text{km}^{-1}$ (Fig. 8a), and for all days with an SBJ, $\alpha = 1.6\ \text{km}^{-1}$ (Fig. 8b). These values are similar to PRISM and the annual averages shown in Fig. 3. However, the OPG differs between high- and low-SBJ days, ranging from $\alpha = 1.1\ \text{km}^{-1}$ (Fig. 8c) to $\alpha = 2.2\ \text{km}^{-1}$ (Fig. 8d), with the largest differences observed at stations

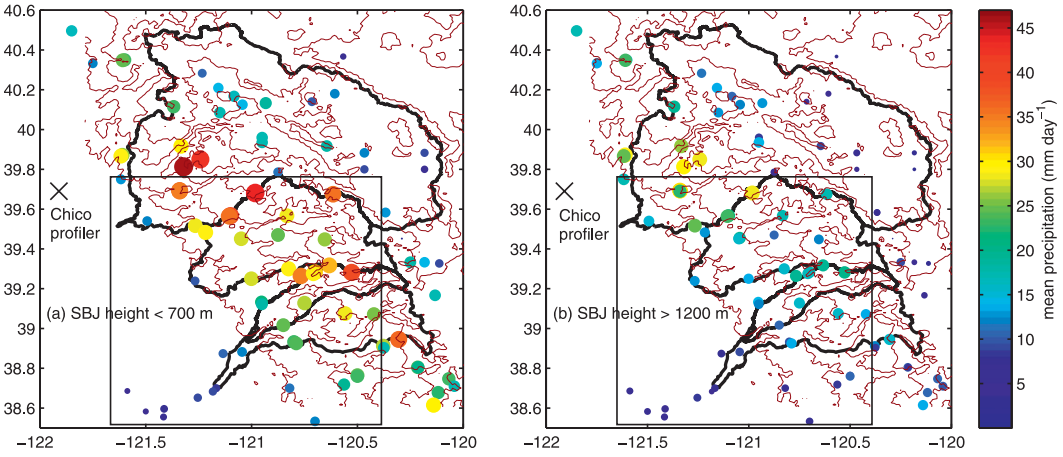

FIG. 7. Average daily precipitation on days with (a) identified SBJs with core altitudes less than 700 m and (b) identified SBJs with core altitudes higher than 1200 m. The × identifies the location of the Chico profiler where the height of the SBJ was determined. Contours show elevation at 500-m intervals. Box identifies subset of stations shown in subsequent plots of precipitation vs elevation.

above 1000 m. To test the statistical significance of this OPG difference, we assembled 1000 sets of 56 days, (the smallest subset used in Fig. 8), chosen randomly from the 424 days with greater than 5 mm of region-mean precipitation. For the mean precipitation versus altitude of each set, α [as defined in Eq. (2)] was calculated, and we found α to be near-normally distributed, with a mean of 1.5 km^{-1} and standard deviation of 0.2 km^{-1}. Of the 1000 sets, 3.7% had $\alpha \leq 1.1$ km^{-1}, and 0.6% had $\alpha \geq 2.2$ km^{-1}. This was repeated for the four hourly precipitation stations detailed in Table 1, using a cutoff of 0.2 mm h^{-1} mean precipitation and the hourly start and stop times of the SBJs. The distribution with height was similar to the daily analysis (Fig. 8). Thus, it is unlikely that the differences in OPG between SBJ classes occur by random chance.

To test whether the OPG varies smoothly with SBJ height or in a threshold fashion, we binned the SBJ events into nine classes based on the mean SBJ elevation and calculated α for each (Fig. 9). While the best-fit values of the OPG show a near-linear decrease with SBJ height, 95%-confidence intervals in estimates of the OPG show that the OPG is only statistically different between events with SBJ heights greater than 1200 m and those with SBJ heights less than 1000 m. The greatest OPGs occurred for SBJ heights less than 400 m; however, because the sample size is 2 days, more samples would be needed to verify that this is generally the case.

The enhanced OPG in the 2007 observational annual precipitation data in Fig. 5h is consistent with the observation that a larger fraction of total annual precipitation that year was associated with low SBJs (Fig. 6). Similarly, 2004 had a larger fraction of annual precipitation occurring during high SBJs, and the OPG was less than would be expected according to climatology or PRISM (Fig. 5e). While the 7-yr dataset is too short to draw statistically significant conclusions, the observations in 2004 and 2007 suggest that SBJ-related variations in precipitation distributions can aggregate to annual values.

6. Implications for hydrology: Case study of water years 2006 and 2007

In the Sierra Nevada, the amount of rain contributing to a flood or snow being stored for summer runoff depends critically on both temperature (i.e., the elevation where snow changes to rain and the OPG (i.e., how much precipitation falls both above and below that elevation). Based on results shown so far, the SBJ height is correlated with the OPG. To test the effect that temperature and precipitation distributions have on basin hydrology, we ran a simple hydrologic model, detailed in section 3d, which includes rain and snow, explicitly representing precipitation and temperature variations with elevation. Precipitation was distributed according to four different scenarios: 1) climatology; that is, the average OPG: $\alpha = 1.5$ km^{-1} (Fig. 8a); 2) high-altitude SBJ: $\alpha = 1.1$ km^{-1} (Fig. 8c); 3) low-altitude SBJ: $\alpha = 2.2$ km^{-1} (Fig. 8d); and 4) precipitation distribution varies each day: on days when a high- or low-altitude SBJ is observed at Chico, precipitation is distributed as described in scenario 2 or 3, respectively. When neither is observed, precipitation is distributed according to climatology, scenario 1.

Hydrologic model simulations were run for water years 2006 and 2007 (Fig. 10). Water year 2006 was examined because it contained a hydrologically important and well-documented flood event (Galewsky and

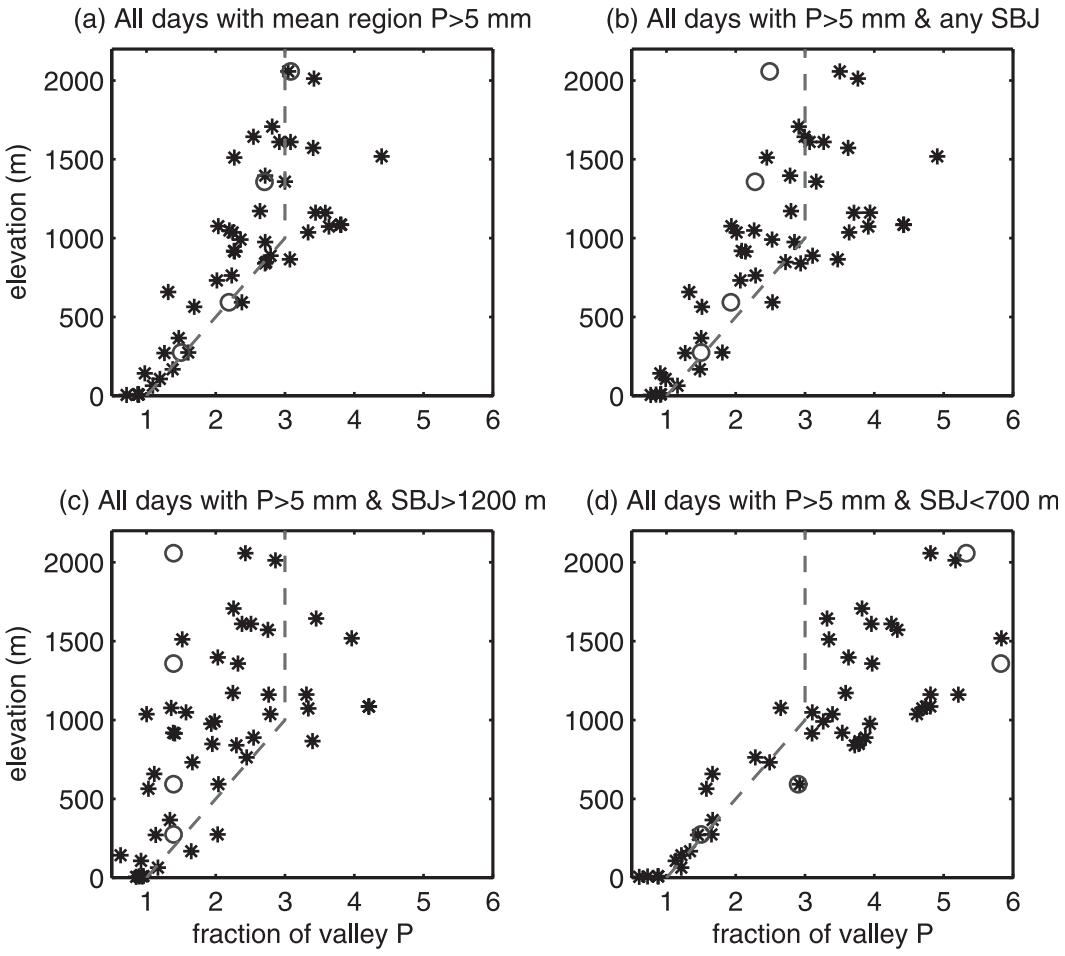

FIG. 8. Average precipitation over (a) all days (424) with mean regional precipitation (P) > 5 mm, (b) all of those days (219) with recognized SBJs, (c) all those days (56) with SBJ heights > 1200 m, and (d) those (67) with SBJ heights < 700 m, as a fraction of average precipitation in the valley (described in text). These valley rates were (a) 8, (b) 10, (c) 10, and (d) 9 mm. Stars represent daily observations. Circles show 1.5 times fractions of Oroville precipitation for the four hourly stations in Table 1, with a mean cutoff of $P > 0.2$ mm h^{-1}. The dashed line identifies the median precipitation rate with elevation described by PRISM for annual accumulation.

Sobel 2005; Reeves et al. 2008; Smith et al. 2010) with warm temperatures and a low-altitude SBJ on 31 December 2005. In addition to the flood, water year 2006 was characterized by a smaller percentage of precipitation at high elevations than average (Fig. 5g). Water year 2007 (Figs. 5h, 6) was examined because it contained a higher percentage of low-altitude SBJs than average, most occurring during cold storms, resulting in a greater fraction of total precipitation deposited at higher elevations, in the snow zone.

The streamflow appears most sensitive to the precipitation distribution during large, warm rainfall events, such as near New Year's 2006 (Figs. 10a,b). Heavy Sierra rainfall is often associated with low-altitude SBJs, which place greater amounts of precipitation at high altitudes. When these events are also warm, as in the New Year's 2006 event, the high-altitude precipitation falls as rain and contributes to runoff, resulting in greater flood peaks than would be expected without the additional orographic enhancement.

Variations in the late-spring and summer snowmelt part of the hydrograph depend on the precipitation distributions during storms cold enough to bring snow. In water year 2006, the simulation with all low-SBJ distributions, with a greater fraction of precipitation at high elevations, accumulated more snow than the simulation with all high-SBJ distributions. This high elevation snow took longer to melt, resulting in simulated streamflow dropping below 5 m^3 s^{-1}, an arbitrary benchmark to represent snow disappearance, 29 days later in the all low-SBJ case than the all high-SBJ distribution. However, when precipitation was distributed by SBJ, on a case-by-case

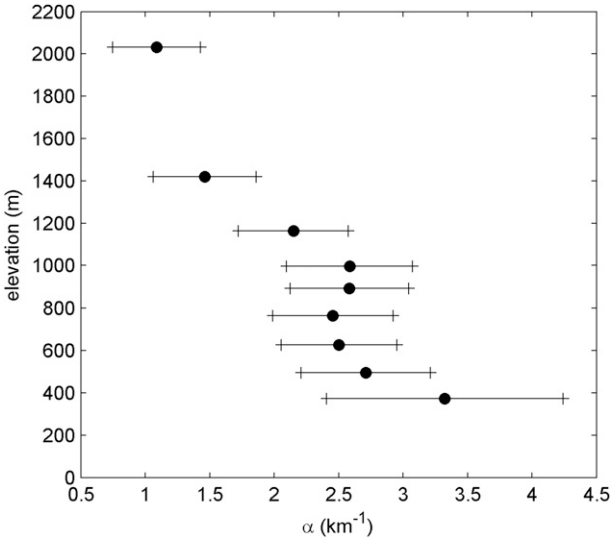

FIG. 9. The normalized OPG, α [as defined in Eq. (2)], as a function of the mean SBJ height. Each dot shown here is the best fit slope of 10 to 20 days with SBJ events, with the exception of the lowest elevation band, which had 2 days, and the second lowest elevation band, which had 8 days. Pluses indicate the extent of 95% confidence intervals in the estimate of α, assuming a normal distribution.

basis, the spring snowmelt timing was only 1 day later than climatology because the higher and lower OPGs balanced each other.

In water year 2007 (Figs. 10c,d), the winter was dry, and spring was warm, such that little snowpack accumulated, and what did accumulate melted early. As in 2006, the low-SBJ-distribution case had greater spring flows from its greater snowpack than the high-SBJ case, but the magnitude of this difference was smaller in 2007 (23 days later for all-low-SBJ flow to drop below 5 $m^3 s^{-1}$) than 2006, because overall it was a drier year. Because 40% of the total precipitation fell on low-SBJ days in 2007, compared to only 10% falling on high-SBJ days (Fig. 6), these two patterns did not completely cancel out in the case-by-case simulation (Fig. 10d). In this case-by-case simulation, simulated streamflow dropped below 5 $m^3 s^{-1}$ four days later than was predicted by climatology.

7. Summary

In regions with water resources dependent on a snowpack (e.g., California), the location and, particularly, the elevation of the deposited snow determines when the snow will melt and the availability of late-summer runoff. Forecasting for water resources relies on statistical relationships between a few point measurements and total basin runoff. These forecasts assume that the spatial relationships are time invariant; that is, the precipitation pattern is the same year after year.

In northern California's Sierra Nevada, spatial storm-by-storm variations, even when aggregated to an annual time scale, cannot be adequately explained by an idealized model of orographic precipitation (Smith and Barstad 2004; LT model) or by monthly PRISM maps of interpolated precipitation. As illustrated in Figs. 7 and 8, variations in the height of a southerly SBJ of wind flowing parallel to the mountain range are associated with changes in the orographic precipitation gradient. The SBJ is not represented in the LT model, and because it often results in patterns that differ from climatology, it is not well-represented in PRISM. The lack of SBJ activity in water year 2001 coincides with a year when the LT model and PRISM best match the patterns of observed precipitation (Fig. 5b), whereas years with over 70% of precipitation falling on days with SBJs (e.g., 2002, 2004, and 2007; Figs. 5, 6) have the worst fit between a linear model, PRISM, and observations. Although seven years is a short time period to draw definite conclusions, this study suggests that SBJ activity may be a primary cause of precipitation patterns deviating from those estimated by an idealized model or PRISM.

We extended the work of Neiman et al. (2010) by examining the spatial patterns of precipitation associated with storms leading to 1) low (altitude < 700 m) and 2) high (altitude > 1200 m) SBJs. Compared to high SBJs, low SBJs are characterized by heavier mountain rain rates and a steeper rate of increase in precipitation with elevation, placing greater relative amounts of precipitation in basin headwaters. In terms of hydrology, the enhanced precipitation increase with elevation is most noticeable in warm storms with low SBJs, such as the New Year's flood of 2006, when heavy precipitation falling at high elevations resulted in more flood runoff than would be predicted by a climatological precipitation distribution. Years with the majority of precipitation falling during low SBJs, such as 2007, would be expected to have a greater fraction of total precipitation falling as snow, and hence, later runoff. The magnitude of this effect depends on the total amount of snow (a wetter year would have a greater relative delay) and the rapidity of spring melt (a cooler spring would have a greater relative delay). In most years, as in 2006, a similar fraction of high- and low-SBJ storms over the year result in spring and summer runoff similar to that predicted using a climatological precipitation pattern.

8. Discussion and conclusions

While our results show that the LT model is able to represent the general effects of wind speed and stability on the OPG through its representation of linear mountain wave dynamics (see Fig. 4), our results also show

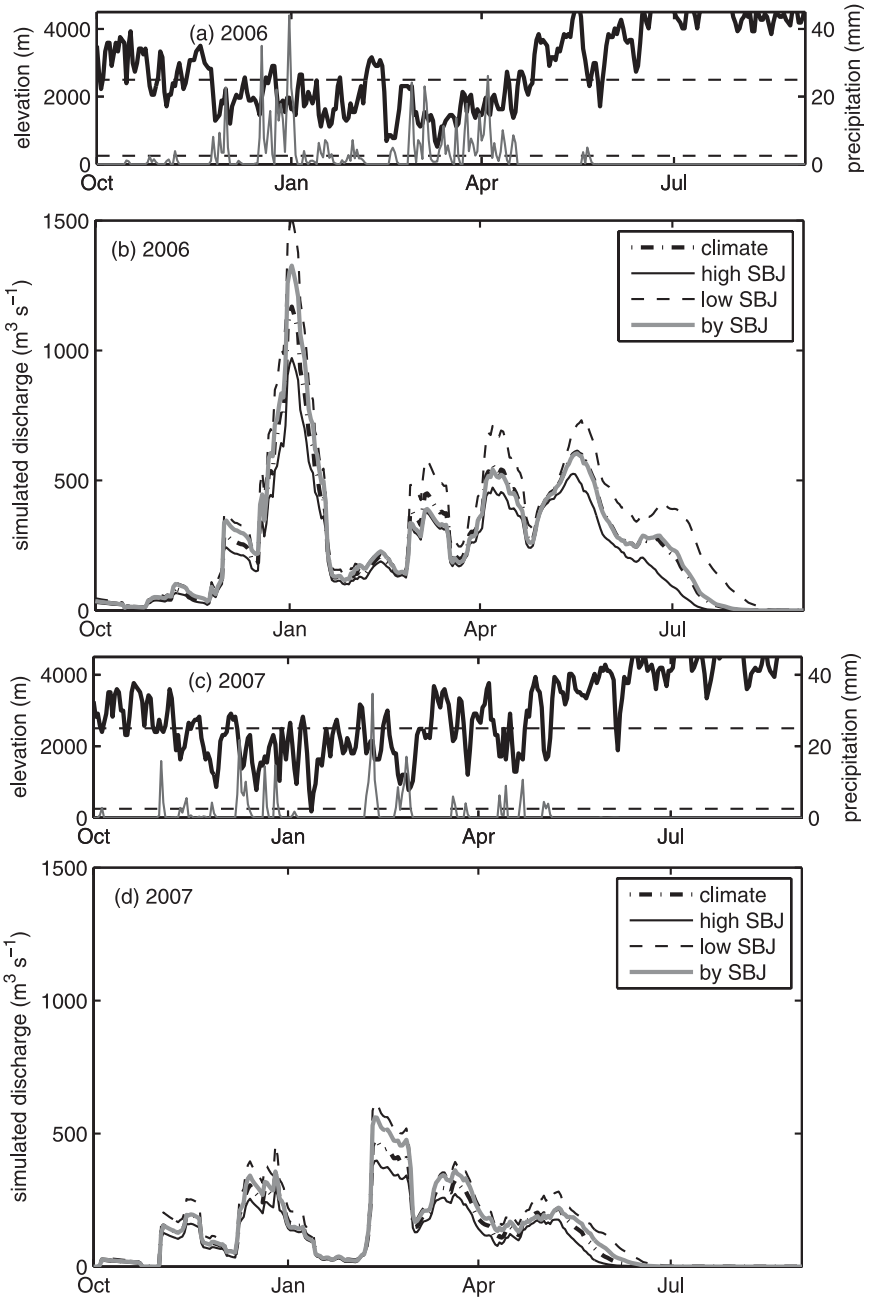

FIG. 10. For (a) 2006 and (c) 2007, elevation where snow changes to rain (1°C isotherm, heavy black line, left axis) and daily reference precipitation (thin gray line, right axis). Horizontal dashed lines indicate the elevation range spanned by the Yuba basin. This information is used to simulate Yuba basin streamflow using four methods of distributing precipitation for water years (b) 2006 and (d) 2007: PRISM climatology (thick dash–dot line), the distribution observed during high altitude barrier jets (thin solid line), the distribution observed during low-altitude barrier jets (thin dashed line), and according to the daily Chico profiler observation of high, low, or neither SBJ type each day, as described in text (thick gray line).

that the model is unable to capture the large OPG variability that is related to SBJ height (see Fig. 5). The failure of the LT model to capture these variations may be related to its inability to represent the effects of nonlinear airflow dynamics that lead to blocking and support SBJ formation (e.g., Hughes et al. 2009). Previous studies have shown that increased blocking leads to a reduction in the OPG by reducing precipitation over

windward slopes and enhancing it well upwind of mountains (e.g., Rotunno and Ferretti 2001; Neiman et al. 2002; Medina and Houze 2003; Galewsky 2008). Insomuch as the SBJ height is an indicator of the extent of blocking, our results broadly agree with these findings. However, these studies have found the extent of blocking, and hence the OPG, to be well characterized by the upstream value of the nondimensional parameter U/N_mH, which is the ratio of cross-barrier wind speed (U) to the buoyancy (N_m) times the mountain height (H). Yet, as shown in Neiman et al. (2010), although all SBJs have upstream U/N_mH values that would indicate blocked flow, these values are not significantly different for high- versus low-altitude SBJs. Thus, previous results on how upwind conditions modulate blocking and the OPG relate poorly to our findings.

Neiman et al. (2010) showed that low SBJs are associated with much greater vertical shear in the cross-mountain wind than high SBJs. Thus, shear may be another atmospheric parameter that is important in explaining our results. Studies that focus on U/N_mH often vertically average the observed wind profile (e.g., Hughes et al. 2009) or rely on simulations with vertically uniform winds (e.g., Jiang 2003; Galewsky 2008), thereby discounting the role of shear. However, variations in shear, independent of variations in the vertically averaged winds, may alter the pattern of mountain wave ascent or airflow blocking in ways that affect the OPG (e.g., Colle 2004). Furthermore, strong wind shear also leads to turbulence and overturning cells above the top of the SBJ, which may promote hydrometeor growth, enhance precipitation over the windward slopes, and affect the OPG (e.g., Houze and Medina 2005; Medina et al. 2005). To better understand the interaction of these effects, future studies should focus on the role of shear in the development of SBJs and the shaping of orographic precipitation patterns.

Both PRISM and a linear model are able to explain the mean OPG and some, but not all, of the variations of the OPG in the northern Sierra. Thus, a full mesoscale model with the ability to accurately represent SBJ characteristics and associated circulations, such as that used by Reeves et al. (2008), is likely required to capture variations in the OPG in this region. However, if turbulence (as in Medina et al. 2005) is the primary mechanism responsible for these patterns, even a full mesoscale model may not be able to represent the small-scale processes involved.

While the altitude of the SBJ is not correlated with freezing level, our results also imply that studies of how long-term climate shifts impact the hydrology of this region need to examine changes in the frequency of storm types that result in high versus low SBJs, as the resulting OPG changes will impact flood magnitudes during warm, wet storms and change how precipitation is distributed with elevation and hence, as rain versus snow.

Acknowledgments. This work was primarily supported by the NOAA HMT project. JDL acknowledges support from NOAA Grant NA17RJ1232 and NSF Grant EAR-0838166. JRM acknowledges support from NSF Grant EAR-0642835. The authors thank the dedicated NOAA/ESRL staff who installed the radar profiler. In addition, we thank the CADWR and cooperators for providing daily and hourly precipitation records across the region and Noah Knowles for automating the downloading of CDEC data and making it available. Finally, thank you to Editor Barros and three anonymous reviewers for their helpful comments and to Mark Raleigh, Jeff Deems, Steve Burges, and Andrey Shcherbina for scientific conversations regarding this material.

REFERENCES

Alpert, P., 1986: Mesoscale indexing of the distribution of orographic precipitation over high mountains. *J. Climate Appl. Meteor.,* **25,** 532–545.

——, and H. Shafir, 1989: Meso-scale distribution of orographic precipitation: Numerical study and comparison with precipitation derived from radar measurements. *J. Appl. Meteor.,* **28,** 1105–1117.

Anders, A. M., G. H. Roe, D. R. Durran, and J. R. Minder, 2007: Small-scale spatial gradients in climatological precipitation on the Olympic Peninsula. *J. Hydrometeor.,* **8,** 1068–1081.

Anderson, E. A., 1973: National weather service river forecast system/snow accumulation and ablation model. U.S. Department of Commerce NOAA Tech. Memo. NWS HYDRO-17, 217 pp.

Barros, A. P., and D. P. Lettenmaier, 1993: Dynamic modeling of the spatial distribution of precipitation in remote mountainous areas. *Mon. Wea. Rev.,* **121,** 1195–1214.

——, and ——, 1994: Dynamic modeling of orographically induced precipitation. *Rev. Geophys.,* **32,** 265–284.

Barry, R. G., 2008: *Mountain Weather and Climate*. 3rd ed. Cambridge University Press, 506 pp.

Barstad, I., and R. B. Smith, 2005: Evaluation of an orographic precipitation model. *J. Hydrometeor.,* **6,** 85–99.

Carter, D. A., K. S. Gage, W. L. Ecklund, W. M. Angevine, P. E. Johnston, A. C. Riddle, J. S. Wilson, and C. R. Williams, 1995: Developments in UHF lower tropospheric wind profiling at NOAA's Aeronomy Laboratory. *Radio Sci.,* **30,** 997–1001.

Colle, B. A., 2004: Sensitivity of orographic precipitation to changing ambient conditions and terrain geometries: An idealized modeling perspective. *J. Atmos. Sci.,* **61,** 588–606.

——, and C. F. Mass, 1998: Windstorms along the western side of the Washington Cascade Mountains. Part II: Characteristics of past events and three-dimensional idealized simulations. *Mon. Wea. Rev.,* **126,** 53–71.

Colton, D. E., 1976: Numerical simulation of the orographically induced precipitation distribution for use in hydrologic analysis. *J. Appl. Meteor.,* **15,** 1241–1251.

Crochet, P., T. Johannesson, T. Jonsson, O. Sigurdsson, H. Bjonsson, F. Palsson, and I. Barstad, 2007: Estimating the spatial distribution of precipitation in Iceland using a linear model of orographic precipitation. *J. Hydrometeor.,* **8,** 1285–1306.

Daly, C., P. Neilson, and D. L. Phillips, 1994: A statistical-topographic model for mapping climatological precipitation over mountainous terrain. *J. Appl. Meteor.,* **33,** 140–158.

——, W. P. Gibson, G. H. Taylor, G. L. Johnson, and P. Pasteris, 2002: A knowledge-based approach to the statistical mapping of climate. *Climate Res.,* **22,** 99–113.

——, M. Halbleib, J. I. Smith, W. P. Gibson, M. K. Doggett, G. H. Taylor, J. Curtis, and P. P. Pasteris, 2008: Physiographically sensitive mapping of climatological temperature and precipitation across the conterminous United States. *Int. J. Climatol.,* doi:10.1002/joc.1688.

Dettinger, M., K. Redmond, and D. Cayan, 2004: Winter orographic precipitation ratios in the Sierra Nevada—Large-scale atmospheric circulations and hydrologic consequences. *J. Hydrometeor.,* **5,** 1102–1116.

Dooge, J., 1973: Linear theory of hydrologic systems. Tech. Bull. 1468, Agricultural Research Service, U.S. Department of Agriculture, 327 pp.

Dunn, L. B., 1992: Evidence of ascent in a sloped barrier jet and an associated heavy-snow band. *Mon. Wea. Rev.,* **120,** 914–924.

Durran, D. R., and J. B. Klemp, 1982: On the effects of moisture on the Brunt-Vaisala frequency. *J. Atmos. Sci.,* **39,** 2152–2158.

Galewsky, J., 2008: Orographic clouds in terrain-blocked flows: An idealized modeling study. *J. Atmos. Sci.,* **65,** 3460–3478.

——, and A. Sobel, 2005: Moist dynamics and orographic precipitation in northern and central California during the New Year's flood of 1997. *Mon. Wea. Rev.,* **133,** 1594–1612.

Hay, L. E., and G. J. McCabe, 1998: Verification of the Rhea-Orographic-Precipitation model. *J. Amer. Water Resour. Assoc.,* **34,** 103–112.

Heggli, M. F., and R. M. Rauber, 1988: The characteristics and evolution of supercooled water in wintertime storms over the Sierra Nevada: A summary of microwave radiometric measurements taken during the Sierra Cooperative Pilot Project. *J. Appl. Meteor.,* **27,** 989–1015.

Houze, R. A., 1993: *Cloud Dynamics*. Academic Press, 570 pp.

——, and S. Medina, 2005: Turbulence as a mechanist for orographic precipitation enhancement. *J. Atmos. Sci.,* **62,** 3599–3623.

Hughes, M., A. Hall, and R. G. Fovell, 2009: Blocking in areas of complex topography and its influence on rainfall distribution. *J. Atmos. Sci.,* **66,** 508–518.

Jeton, A. E., M. D. Dettinger, and J. LaRue Smith, 1996: Potential effects of climate change on streamflow, eastern and western slopes of the Sierra Nevada, California and Nevada. USGS Water Resources Investigations Rep. 95-4260, 44 pp.

Jiang, Q., 2003: Moist dynamics and orographic precipitation. *Tellus,* **55A,** 301–316.

——, and R. Smith, 2003: Cloud timescales and orographic precipitation. *J. Atmos. Sci.,* **60,** 1543–1559.

Knowles, N., M. D. Dettinger, and D. R. Cayan, 2006: Trends in snowfall versus rainfall in the western United States. *J. Climate,* **19,** 4545–4559.

Leung, L. R., and S. J. Ghan, 1995: A subgrid parameterization of orographic precipitation. *Theor. Appl. Climatol.,* **52,** 95–118.

——, and ——, 1998: Parameterizing subgrid orographic precipitation and surface cover in climate models. *Mon. Wea. Rev.,* **126,** 3271–3291.

——, M. S. Wigmosta, S. J. Ghan, D. J. Epsein, and L. W. Vail, 1996: Application of a subgrid orographic precipitation/surface hydrology scheme to a mountain watershed. *J. Geophys. Res.,* **101** (D8), 12 803–12 817.

Loescher, K. A., G. S. Young, B. A. Colle, and N. S. Winstead, 2006: Climatology of barrier jets along the Alaskan coast. Part I: Spatial and temporal distributions. *Mon. Wea. Rev.,* **134,** 437–453.

Lundquist, J. D., P. J. Neiman, B. Martner, A. B. White, D. J. Gottas, and F. M. Ralph, 2008: Rain versus snow in the Sierra Nevada, California: Comparing radar and surface observations of melting level. *J. Hydrometeor.,* **9,** 194–211.

Martner, B. E., and Coauthors, 1993: An evaluation of wind profiler, RASS, and microwave radiometer performance. *Bull. Amer. Meteor. Soc.,* **74,** 599–613.

Marwitz, J., 1983: The kinematics of orographic airflow during Sierra storms. *J. Atmos. Sci.,* **40,** 1218–1227.

Medina, S., and R. A. Houze Jr., 2003: Air motions and precipitation growth in alpine storms. *Quart. J. Roy. Meteor. Soc.,* **129,** 345–371.

——, B. F. Smull, R. A. Houze, and M. Steiner, 2005: Cross-barrier flow during orographic precipitation events: Results from MAP and IMPROVE. *J. Atmos. Sci.,* **62,** 3580–3598.

Miller, N. L., and J. Kim, 1996: Numerical prediction of precipitation and river flow over the Russian River watershed during the January 1995 California storms. *Bull. Amer. Meteor. Soc.,* **77,** 101–105.

Minder, J. R., 2010: The sensitivity of mountain snowpack accumulation to climate warming. *J. Climate,* **23,** 2634–2650.

Neiman, P. J., F. M. Ralph, A. B. White, D. E. Kingsmill, and P. O. G. Persson, 2002: The statistical relationship between upslope flow and rainfall in California's coastal mountains: Observations during CALJET. *Mon. Wea. Rev.,* **130,** 1468–1492.

——, E. M. Sukovich, F. M. Ralph, and M. Hughes, 2010: A seven-year wind profiler-based climatology of the windward barrier jet along California's northern Sierra Nevada. *Mon. Wea. Rev.,* **138,** 1206–1233.

Pandey, G. R., D. R. Cayan, and K. P. Geogakakos, 1999: Precipitation structure in the Sierra Nevada of California during winter. *J. Geophys. Res.,* **104** (D10), 12 019–12 030.

Parish, T. R., 1982: Barrier winds along the Sierra Nevada Mountains. *J. Appl. Meteor.,* **21,** 925–930.

Petersen, G. N., J. E. Kristjansson, and H. Olafsson, 2005: The effect of upstream wind on airflow in the vicinity of a large mountain. *Quart. J. Roy. Meteor. Soc.,* **131,** 1113–1128.

Pierrehumbert, R. T., and B. Wyman, 1985: Upstream effects of mesoscale mountains. *J. Atmos. Sci.,* **42,** 977–1003.

Queney, P., 1947: Theory of perturbations in stratified currents with applications to airflow over mountain barriers. Dept. of Meteorology, University of Chicago, Miscellaneous Rep. 23, 81 pp.

Ralph, F. M., and Coauthors, 2005: Improving short term (0–48 hour) cool season quantitative precipitation forecasting: Recommendations from an USWRP workshop. *Bull. Amer. Meteor. Soc.,* **86,** 1619–1632.

Reeves, H. D., Y.-L. Lin, and R. Rotunno, 2008: Dynamic forcing and mesoscale variability of heavy precipitation events over the Sierra Nevada Mountains. *Mon. Wea. Rev.,* **136,** 62–77.

Reiter, E. R., 1963: *Jet-Stream Meteorology*. University of Chicago Press, 515 pp.

Rhea, J. O., 1978: Orographic precipitation model for hydrometeorological use. Colorado State University Atmospheric Paper 287, 198 pp.

——, and L. O. Grant, 1974: Topographic influences on snowfall patterns in mountainous terrain. *Proc. Symp. on Advanced Concepts and Techniques in the Study of Snow and Ice Resources,* Monterey, CA, National Academy of Sciences, 182–192.

Roe, G. H., 2002: Modeling precipitation over ice sheets: An assessment using Greenland. *J. Glaciol.,* **48,** 70–80.

——, 2005: Orographic precipitation. *Annu. Rev. Earth Planet. Sci.,* **33,** 645–671.

——, and M. B. Baker, 2006: Microphysical and geometrical controls on the pattern of orographic precipitation. *J. Atmos. Sci.,* **63,** 861–880.

Rotunno, R., and R. Ferretti, 2001: Mechanisms of intense alpine rainfall. *J. Atmos. Sci.,* **58,** 1732–1749.

Sawyer, J. S., 1956: The physical and dynamical problems of orographic rain. *Weather,* **11,** 375–381.

Shutts, G. J., 1998: Idealized models of the pressure drag force on mesoscale mountain ridges. *Contrib. Atmos. Phys.,* **71,** 303–315.

Sinclair, M. R., 1994: A diagnostic model for estimating orographic precipitation. *J. Appl. Meteor.,* **33,** 1163–1175.

Smith, B. L., S. E. Yuter, P. J. Neiman, and D. E. Kingsmill, 2010: Water vapor fluxes and orographic precipitation over Northern California associated with a land-falling atmospheric river. *Mon. Wea. Rev.,* **138,** 74–100.

Smith, R. B., 1979: The influence of mountains on the atmosphere. *Adv. Geophys.,* **21,** 87–230.

——, 1989: Mountain-induced stagnation points in hydrostatic flow. *Tellus,* **41A,** 270–274.

——, 2002: Stratified airflow over topography. *Environmental Stratified Flows,* R. Grimshaw, Ed., Vol. 3, *Topics in Environmental Fluid Mechanics,* Kluwer, 119–159.

——, 2003: A linear upslope-time-delay model for orographic precipitation. *J. Hydrol.,* **282,** 2–9.

——, and I. Barstad, 2004: A linear theory of orographic precipitation. *J. Atmos. Sci.,* **61,** 1377–1391.

——, and Coauthors, 2003: Orographic precipitation and air mass transformation: An Alpine example. *Quart. J. Roy. Meteor. Soc.,* **129,** 433–454.

Smutz, S. W., 1986: A climatology of the Sierra Nevada barrier jet. M.S. thesis, Dept. of Atmospheric Science, University of Wyoming, 108 pp.

Stewart, I. T., D. R. Cayan, and M. D. Dettinger, 2005: Changes towards earlier streamflow timing across western North America. *J. Climate,* **18,** 1136–1155.